Acta Cryst. (1984). B40, 484–492

The Static Deformation Density of Tetrafluoroterephthalonitrile (TFT) from the Zürich X-ray Data at 98 K

BY F. L. HIRSHFELD

Department of Structural Chemistry, The Weizmann Institute of Science, Rehovot 76100, Israel

(*Received* 1 *March* 1984; *accepted* 11 *May* 1984)

Dedicated to Professor Jack D. Dunitz on the occasion of his 60th birthday

Abstract

The low-temperature X-ray data for TFT measured by Dunitz and coworkers have led, *via* multipole refinement, to a static deformation density map. In support of the data and the model, final discrepancy indices are $R = 0{\cdot}036$, $R_w(F^2) = 0{\cdot}019$, GOF = 1·140, the discrepancies ΔF show negligible systematic trends and yield a residual density showing mainly random noise, vibration parameters satisfy the rigid-bond test, and the total electron density is everywhere positive. Results accord well with the high-order refinement of Dunitz *et al.* The deformation density closely resembles experimental and theoretical maps of related molecules. Both π-conjugative and σ-inductive effects seem responsible for unequal aromatic bond lengths and angles. Partitioned atomic moments for the C≡N and C–F fragments approximately match corresponding quantities from two other X-ray and six SCF studies. The small C–F bond peak does not provide the electrostatic binding required by the Hellmann–Feynman theorem; this must come mainly from an undetectable forward polarization in the core region around *F*.

Introduction

The low-temperature X-ray diffraction data for tetrafluoroterephthalonitrile, $C_6F_4(CN)_2$, measured by Dunitz and coworkers (Dunitz, Schweizer & Seiler, 1982; Seiler, Schweizer & Dunitz, 1984) [DSS (1982) and SSD (1984) hereafter] have been extensively tested and appear to be of exceptionally high quality. They have led to dynamic deformation density maps of more than routine chemical interest. It thus appeared likely that a static deformation map derived from these data would permit even clearer and more decisive chemical interpretation.

On the strength of a careful analysis by SSD (1984) of alternative data-reduction procedures, their revised data set DP2 was chosen for the present study. The data comprise 2387 net intensities I_o, 208 of them negative, with their estimated standard deviations, measured at 98 K and extending to reciprocal radius $S = 2\sin\theta/\lambda = 2{\cdot}30$ Å^{-1}. They served as input for least-squares refinement, on F^2, with the deformation refinement program *LSEXP* (Hirshfeld, 1977*a*). In addition to a scale factor, isotropic-extinction parameter, and atomic coordinates and anisotropic harmonic vibration parameters, effectively 82 charge-density parameters were refined. These comprised exponential factors α_a (for the multipole functions with $n > 0$) for the five independent atoms and 78 coefficients of the multipole functions

$$\rho_{a,k}(r_a) = N_n r_a^n \exp(-\alpha_a r_a)\cos^n\theta_k$$

centered on these atoms: 22 for atom C(1), constrained to local symmetry *m*, and 14 each for the other four atoms, constrained to *mm* symmetry, reduced by one neutrality constraint as described by Harel & Hirshfeld (1975). The cusp functions $\rho_{a,0} = N_0 \exp(-\alpha_{a,0} r_a)$ were assigned exponential factors $\alpha_{a,0} = 2Z_a/a_0$ (Eisenstein, 1979).

Internal tests of the refinement

This deformation model has led to discrepancy indices $R = 0{\cdot}036$ (0·028 excluding negative intensities), $R_w(F^2) = 0{\cdot}019$, GOF = 1·140;* the first and last of these quantities may be compared with 0·055 and 4·764, respectively, for a spherical-atom refinement on the same data (SSD, 1984). Mean discrepancies $\Delta|F|$ and weighted mean-square discrepancies $w(\Delta F^2)^2$, averaged over small intervals in *F* or in *S*, show no conspicuous systematic trends. However, a slight tendency to negative differences $\Delta|F|$ for the weakest reflections implies that these reflections may have been systematically underestimated (see SSD), especially as the trend persists when the reflections are sorted according to F_c rather than F_o. The pattern seems to be somewhat clearer in terms of *I* (Fig. 1), *i.e.* before correction for Lorentz and polarization factors. Note that for the first two groups in Fig. 1, comprising 194 reflections with $I_c < 0{\cdot}16$,

* Lists of structure factors have been deposited with the British Library Lending Division as Supplementary Publication No. SUP39455 (7 pp.). Copies may be obtained through The Executive Secretary, International Union of Crystallography, 5 Abbey Square, Chester CH1 2HU, England.

0108-7681/84/050484-09$01.50

the mean value of I_o is negative, *i.e.* the measured reflection intensity is, on average, below background. Also, while weak reflections are most numerous at high angles, the same bias is evident at all reciprocal radii.

A residual density map (Fig. 2) evaluated from the full set of Fourier coefficients ΔF (except 84 terms with $|F_c| < F_o/2$, omitted because of uncertain signs; F_o taken as zero when $I_o < 0$) shows largely random noise, whose most prominent features do not exceed $\pm 0{\cdot}3$ e Å^{-3}. Much of this noise is attributable to a minority of imprecisely measured reflections that had small weights in the least-squares refinement but that contribute fully to the Fourier sum. However, all atomic centers are at positions of negative $\Delta\rho$, ranging from $-0{\cdot}07$ to $-0{\cdot}20$ e Å^{-3}, evidently a real-space expression of the negative bias in F_o for many weak reflections.

The rigid-bond test (Hirshfeld, 1976) shows an r.m.s. discrepancy of 0·00013 Å^2 for the four pairs of non-equivalent bonded atoms (Table 1). This is comparable with the estimated standard deviations of the diagonal U^{ii} components, which range from 0·00004 to 0·00021 Å^2 (Table 2). For non-bonded pairs, the largest differences are 0·00094 Å^2 for C(3)···F and 0·00089 Å^2 for C(1)···N, implying some departure from rigid-body behavior in the in-plane vibrations (Rosenfield, Trueblood & Dunitz, 1978).

The total static density, *i.e.* promolecule plus deformation density, is positive throughout the unit cell.

A further check on the deformation model and on the stability of the solution obtained was provided by a test refinement in which the constraint on the fluorine deformations was relaxed to symmetry *m*, in accordance with the true symmetry of the isolated molecule. With eight additional parameters, convergence proceeded smoothly but the discrepancy indices scarcely decreased, *e.g.* $R_w(F^2)$ dropped from 0·0189 to 0·0188. Most parameter shifts were entirely insignificant and none exceeded 1·8 times its (new) estimated standard deviation. All indications thus support the *mm* constraint, which conforms to the local symmetry as far as second-nearest neighbors of the F atom. The deformations on C(1) also obey *mm* symmetry within 2σ although no such constraint was ever imposed.

Table 1. *Mean-square displacements* ($\times 10^5$, Å^2) *of atom pairs A, B along their internuclear vector*

The first four pairs listed denote covalent bonds. (See Fig. 3 for atom numbering.)

A	B	z_A^2	z_B^2	A	B	z_A^2	z_B^2
C(1)	C(2)	1025	1020	C(1)	N	963	1052
C(2)	C(3)	768	785	F	N	1697	1762
C(1)	F	859	844	C(1′)	C(2)	827	852
C(3)	N	785	796	C(1′)	C(3)	842	885
C(1)	C(3)	991	1017	C(1′)	F	991	1017
C(2)	F	1107	1128	C(2′)	F	911	903
C(3)	F	1474	1569	C(1″)	F	989	977

It is of some interest that stable convergence has been achieved despite correlation coefficients ranging up to 0·95 between deformation parameters and atomic coordinates. (Correlations up to 0·99 between deformation coefficients are of far less concern as these coefficients have, individually, no physical meaning.) Such strong correlations evidently reflect the sharpness of some deformation features, as indicated by the exponential factors $\alpha_N = 8{\cdot}4\,(8)$ and $\alpha_F = 9{\cdot}8\,(9)$ Å^{-1} (not to mention the cusp exponents $\alpha_{N,0} = 26{\cdot}5$, $\alpha_{F,0} = 34{\cdot}0$ Å^{-1}), compared with values of 5·2 to 7·0 Å^{-1} for the several C atoms. They should warn us that appreciable deformation effects persist in the X-ray data out to the largest reciprocal radii, making even a high-order refinement, with a spherical-atom model, subject to likely bias (see below). In fact the relative average contribution of the deformation terms to the calculated structure factors $\langle|F_{def}|\rangle/\langle|F_c|\rangle$ declines very gradually from 0·04 at low reciprocal radii to 0·02 at $S = 2{\cdot}3$ Å^{-1} (0·01 without cusp functions). Apparently, there are exceptions to the common supposition that deformation scattering is confined to low Bragg angles.

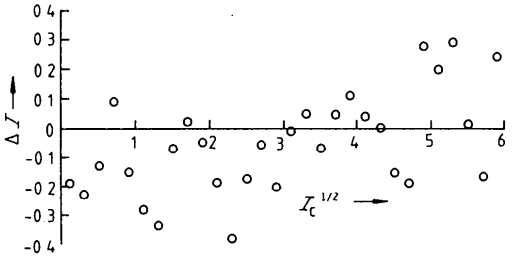

Fig. 1. $\langle\Delta I\rangle = \langle I_o - I_c\rangle$, where I_o is scaled by k^{-2} (but uncorrected for Lorentz–polarization factor Lp), $I_c = \mathrm{Lp}F_c^2$, averaged over intervals of 0·2 in $I_c^{1/2}$, for the 1705 reflections with $I_c < 36$. Note: the number of reflections per interval decreases with increasing I_c from ~100 to ~25 over the range plotted.

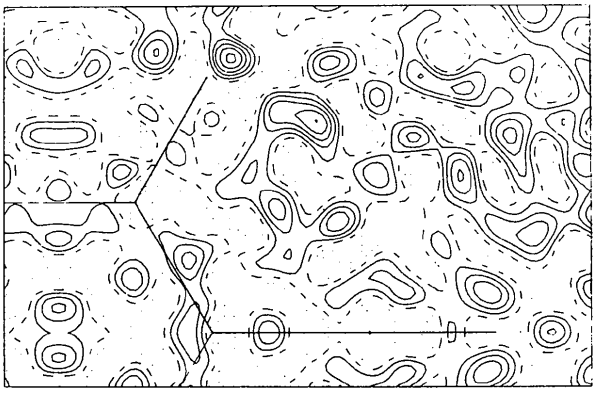

Fig. 2. Residual difference density in mean molecular plane, based on 2303 Fourier coefficients ΔF for which $|F_c| > F_o/2$ ($\Delta F = -F_c$ when $I_o < 0$). Contour interval 0·05 e Å^{-3}.

Table 2. *Refined atomic coordinates* ($\times 10^5$) *and vibration parameters* ($\times 10^5$, Å^2), *with estimated standard deviations in the last digit*

	C(1)	C(2)	C(3)	F	N
x	15652 (3)	0	0	30591 (5)	0
y	5912 (2)	11982 (2)	24203 (4)	11510 (2)	34126 (7)
z	4020 (1)	8086 (2)	16327 (3)	7925 (2)	22944 (5)
U^{11}	957 (4)	1107 (8)	1745 (11)	1111 (10)	2969 (21)
U^{22}	933 (5)	803 (6)	928 (11)	1642 (10)	1212 (10)
U^{33}	1061 (4)	929 (6)	1043 (9)	1796 (10)	1546 (11)
U^{12}	−86 (4)	0	0	−353 (5)	0
U^{23}	−85 (3)	−81 (4)	−193 (8)	−270 (6)	−564 (8)
U^{13}	−44 (3)	0	0	−199 (3)	0

Table 3. *Bond lengths* (Å) *from SSD (spherical-atom model) using all data and high-order* ($S > 1{\cdot}7$ Å^{-1}) *data and from present deformation model*

Last column gives values corrected for vibration (libration only for first four bonds, libration plus bending for C≡N).

	Spherical atom		Deformation	
Bond	All data	High-order	Refined	Corrected
C(1)–C(1′)	1·3814	1·3841	1·3839	1·3850
C(1)–C(2)	1·3918	1·3950	1·3953	1·3973
C(2)–C(3)	1·4322	1·4270	1·4267	1·4279
C(1)–F	1·3313	1·3264	1·3244	1·3263
C(3)–N	1·1489	1·1538	1·1545	1·1580

Molecular dimensions and vibrational motion

Refined atomic coordinates and vibration parameters are listed in Table 2, while Fig. 3 shows the corresponding molecular dimensions. Table 3 compares the uncorrected bond lengths with those derived by SSD, with a spherical-atom model, from all 2387 reflections and from the 1406 reflections at $S > 1{\cdot}7$ Å^{-1}. The latter results are seen to agree closely with the present bond lengths and to fall, with one minor exception, between these and the values from the full-data spherical-atom refinement. A plausible interpretation is that the multipole deformation model has removed somewhat more of the spherical-atom bias in atomic positions than has the high-order refinement of SSD.

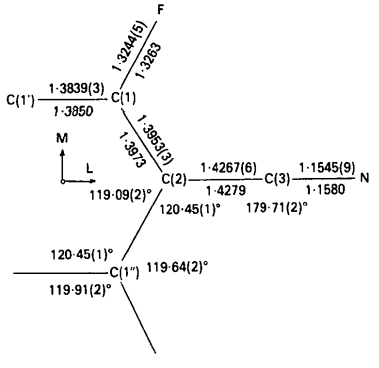

Fig. 3. Molecular dimensions, with estimated standard deviations in parentheses. Bond lengths (Å): uncorrected above the bond axis, corrected below.

Table 4. *Rigid-body tensor components* T^{ij} ($\times 10^5$, Å^2) *and* L^{ij} ($\times 10^6$, rad^2) *referred to crystal axes, fitted to atoms* C(1), C(2), C(3), F *and constrained to* 2/*m site symmetry*

ij	11	22	33	23
T^{ij}	881 (2)	752 (2)	816 (3)	−20 (2)
L^{ij}	461 (8)	1671 (8)	1542 (6)	399 (6)

The vibration parameters show a rather less consistent pattern. The present values (Table 2) are mostly close to those obtained by SSD from the high-order data, with a very slight tendency to smaller amplitudes. The largest differences seem consistent with a spherical-atom bias in the high-order refinement but the relation is not unequivocal.

The vibrational analysis performed by DSS (1982) found the benzene ring and atoms directly bonded to it to behave as a fairly rigid body but revealed in-plane bending vibration of the C≡N bonds with an r.m.s. amplitude of 2·2°. This model fitted the refined atomic U^{ij} parameters with an r.m.s. deviation of 0·00044 Å^2. On the expectation that out-of-plane bending should be as free as in-plane bending, we have removed the N atom completely from the rigid-body constraint. The molecular translation and libration parameters were not fitted to the independently derived atomic vibration components but were introduced directly into the least-squares refinement against the X-ray data. Thus, the vibration components U^{ij} of atoms C(1), C(2), C(3), and F were made dependent on the eight symmetry-allowed components of the rigid-body tensors **T** and **L**, while all other parameters, including the vibration parameters of atom N, were fixed at the values obtained in the unconstrained refinement. This procedure caused $R_w(F^2)$ to increase from 0·0189 to 0·0244 and yielded the rigid-body tensor components listed in Table 4. The corresponding vibration parameters for the four constrained atoms differ from the respective unconstrained values (Table 2) by an r.m.s. difference of 0·00034 Å^2, several times the r.m.s. estimated standard deviation of 0·00007 Å^2. Thus the deviations from rigid-body behavior are small but probably real. One such deviation, supported by the data in Table 1, appears to involve in-plane bending of the C—F bond, but a detailed analysis of such internal vibrations is not possible from the X-ray evidence alone. For the N atom, the unconstrained vibration parameters exceed those evaluated from the rigid-body parameters of Table 4 by 0·00042 Å^2 along the C≡N bond, 0·00165 Å^2 in the plane and perpendicular to the bond, and 0·00418 Å^2 perpendicular to the molecular plane. The latter two quantities correspond to apparent bending motions of the C≡N bond with r.m.s. amplitudes of 2·02° in the plane and 3·21° out of the plane.

The last column of Table 3 lists the corrected bond lengths derived from this model. For the C≡N bond, the corrections for libration (0·0010 Å) and for the two bending vibrations (0·0007 and 0·0018 Å) have been applied additively, assuming these motions to be uncorrelated in phase. The total correction of 0·0035 Å may well be an underestimate. From the unconstrained vibration parameters of Table 2 we may derive a correction of 0·0087 Å if we suppose atom N to ride on atom C(3), 0·0341 Å if the motions of the two atoms are totally uncorrelated (Busing & Levy, 1964). Even if we take the riding correction as a plausible upper limit, it is apparent that the uncertainty in the vibration correction for this bond length far exceeds the likely error in the mean atomic positions. Similarly, if we treat atom F as riding on C(1), the correction to the C—F bond length rises from 0·0019 to 0·0061 Å.

Deformation density

Fig. 4 shows the estimated standard deviation $\sigma(\delta\rho)$ of the static deformation density in the mean molecular plane. Except within 0·2 to 0·3 Å of the several atomic centers, $\sigma(\delta\rho)$ is well under 0·1 e Å^{-3}; near the bond midpoints it is mainly under 0·02 e Å^{-3}. We therefore expect that features seen in a deformation density map contoured at 0·1 e Å^{-3} intervals should be highly significant except very close to the nuclear positions. Fig. 5 shows such maps in the mean molecular plane, in the crystallographic mirror plane perpendicular to this, and in perpendicular planes through the C(1′)–C(1), C(1)–C(2), and C(1)–F bonds.

Fig. 6 displays the corresponding dynamic deformation density in the mean molecular plane. This generally agrees well with Fig. 5 of SSD, comprising two X–X Fourier maps from their high-order refinement, but differs from these for three main reasons. Most significantly, the deformation model has greatly enhanced several marginal features near the F atom that are too small and sharply localized to have survived fully the high-order spherical-atom refinement. This difference correlates directly with the small but systematic changes in atomic parameters noted above, especially the 0·002 Å shift in position of the F atom (Table 3). Secondly, Fig. 6 has been derived solely from calculated structure factors and is thus virtually free of noise originating in the measured structure amplitudes. Finally, it has been computed with the full 2·3 Å^{-1} resolution of the X-ray experiment, compared to the 1·7 Å^{-1} resolution of the truncated SSD maps. Most of these differences are further greatly enhanced in the static maps of Fig. 5.

The major peaks and valleys in Fig. 5 (apart from the nuclear regions) show pleasingly detailed agreement in magnitude, position, and shape with similar features found in previous experimental and theoretical studies of other molecules containing analogous chemical fragments. Thus, the overall appearance of the benzene ring closely matches the map derived by Baert, Coppens, Stevens & Devos (1982), using a similar deformation model, for the aromatic ring in pyridinium dicyanomethylide. The C–C≡N chain also resembles the corresponding portion of the same molecule studied by Baert *et al.* (1982) as well as the Hartree–Fock deformation density of cyanogen (Hirshfeld, 1971). The C–F bond region, where, as we have seen, the features found in Fig. 5 depend crucially on the multipole model, is reassuringly

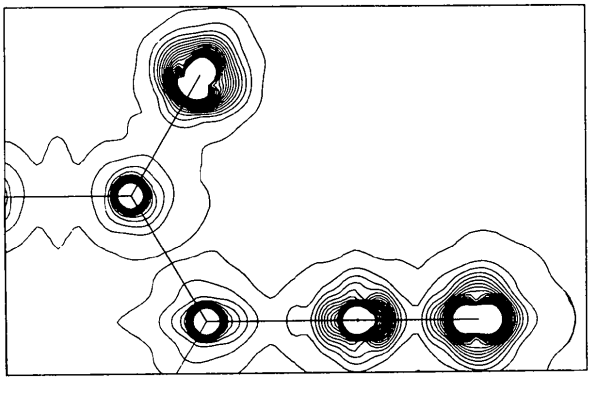

Fig. 4. Estimated standard deviation $\sigma(\delta\rho)$ of the static deformation density in the mean molecular plane, evaluated from the covariance matrix of the refined deformation parameters. Contour interval 0·01 e Å^{-3}, terminated at 0·20 e Å^{-3}.

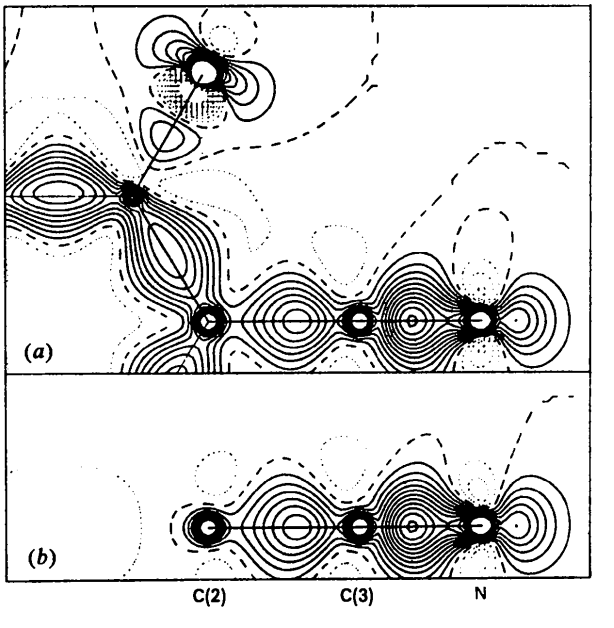

Fig. 5. Static deformation density $\delta\rho$ from the multipole refinement. Contour interval 0·1 e Å^{-3}, terminated at 1·5 e Å^{-3}. (*a*) Mean molecular plane. (*b*) Section at $x = 0$ through C–C≡N group.

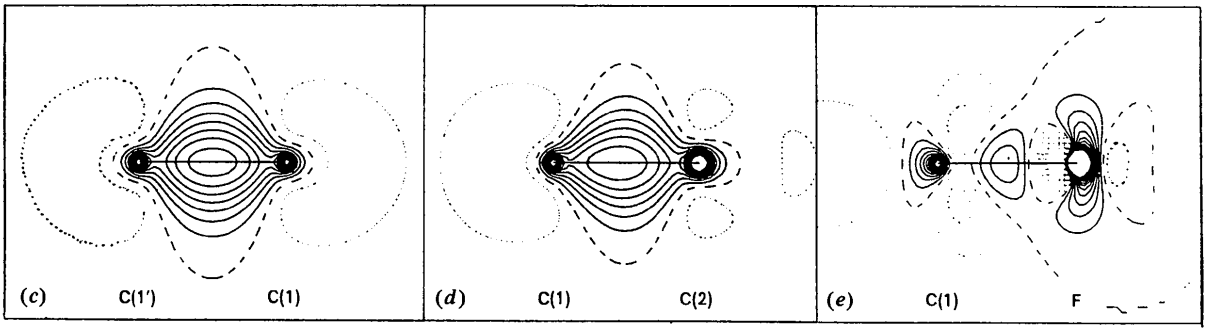

Fig. 5. (*cont.*). (*c*) Perpendicular section through C(1')–C(1) bond. (*d*) Perpendicular section through C(1)–C(2) bond. (*e*) Perpendicular section through C–F bond.

similar to the corresponding region of formyl fluoride as mapped by an extended-basis SCF calculation (Eisenstein & Hirshfeld, 1983). These fairly detailed comparisons provide strong simultaneous support for the accuracy of the X-ray data of Dunitz *et al.*, for the validity of the refinement model used in this study, for the adequacy of the SCF calculations, and for the transferability of deformation density features in the several chemical fragments forming the TFT molecule.

For a more quantitative description of the charge distribution, the molecular deformation density has been partitioned, according to the stockholder recipe (Hirshfeld, 1977*b*), into atomic fragments, which have been integrated numerically to yield atomic net charges and dipole and second moments (Table 5). The integration used an orthogonal 0·1 Å grid extending in each direction 3·0 Å beyond the nearest atom of the asymmetric unit. The last two lines of Table 5 give the moments of the complete molecule. The apparent net charge of +0·003 or +0·009 e is a measure of the error in the numerical integration.

The two sets of moments in Table 5 correspond to alternative definitions of the molecular deformation density. The conventional prescription simply assigns to each molecule the sum of deformation functions centered on the atoms comprising the molecule. This corresponds to what Coppens (1982) has called the pseudomolecule. The alternative definition uses the stockholder recipe for partitioning the crystal into separate molecules (Eisenstein, 1979). This partitioning reassigns some of the deformation density in the region of intermolecular overlap and leads to an overall moderation of the intramolecular charge separation. Thus, the atomic charges all decrease slightly in magnitude, by about 0·01 e. At the same time, the deviations from *mmm* molecular symmetry increase slightly (non-zero atomic moments μ_n, μ_{ln}, and μ_{mn}). But the effects on the individual atomic moments are mainly confined to the last digit given in Table 5 and have no real significance. The largest changes in the second moments are a uniform decrease by 0·021 to 0·025 e Å^2 in μ_{nn} on the three C atoms and smaller positive increments in all three diagonal moments μ_{ii} on N. All these minor changes, however, add up to an appreciable decrease in the magnitudes of the second moments of the molecular deformation density, analogous to the general tendency previously noted in cyanoguanidine (Hirshfeld & Hope, 1980). This ambiguity of definition is evidently a fundamental obstacle to any quantitative derivation of molecular dipole and quadrupole moments by crystallographic methods.

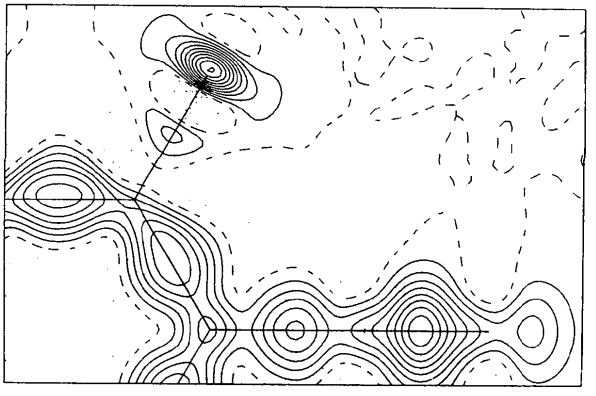

Fig. 6. Dynamic deformation density in mean molecular plane, based on 2387 Fourier coefficients F_{def} calculated from refined multipole parameters. Contour interval 0·1 e Å^{-3}.

Estimated standard deviations for the first definition only (Table 5) have been evaluated from the covariance matrix of the 83 deformation parameters (including the exponents α_a) as outlined by Rees (1977). The requisite integrations were performed on an orthogonal 0·2 Å grid far from the atomic positions and on four interpenetrating 0·2 Å grids, forming a face-centered lattice, within 2 Å of the atomic centers. Comparison of results from the several grids showed this procedure to be adequate for the atomic charges, more than adequate for the outer moments. The largest atomic moments listed in Table 5 are seen to be typically over ten times their respective estimated standard deviations.

Table 5. *Net charges q* ($\times 10^3$, e), *dipole moments* μ_i ($\times 10^3$, e Å), *and second moments* μ_{ij} ($\times 10^3$, e Å^2) *of partitioned atomic deformation densities, referred to orthogonal axes on each atom parallel to molecular inertial axes* **L, M, N** (*see Fig.* 3)

For each atom, first row is based on sum of deformation functions centered on a single molecule (estimated standard deviations in parentheses), second row is based on stockholder partitioning of crystal density. Last two lines give moments of molecular deformation density. Omitted components are exactly or nearly zero by symmetry.

	q	μ_l	μ_m	μ_{ll}	μ_{mm}	μ_{nn}	μ_{lm}
C(1)	126 (9)	40 (5)	55 (7)	93 (6)	104 (7)	200 (16)	−10 (3)
	118	41	56	89	99	177	−12
C(2)	47 (11)	34 (6)	0	110 (7)	95 (7)	189 (18)	0
	39	34	0	105	90	164	0
C(3)	113 (16)	−102 (6)	0	15 (4)	174 (13)	185 (15)	0
	107	−96	0	18	173	164	0
F	−129 (12)	−28 (5)	−53 (4)	7 (5)	11 (5)	11 (4)	−3 (1)
	−122	−22	−48	12	15	17	−6
N	−151 (19)	−12 (11)	0	−51 (8)	12 (9)	22 (8)	0
	−135	5	0	−31	28	33	0
Mol.	3	0	0	−3573	−1340	1637	0
	9	0	0	−2901	−1148	1499	0

Chemical significance

The benzene ring

The two non-equivalent aromatic bonds C(1′)–C(1) and C(1)–C(2) differ in length by over 0·01 Å (Table 3). The room-temperature study of van Rij & Britton (1981) showed a slightly smaller difference of 0·007 Å in the same sense. The obvious explanation is that conjugation with the cyano substituents induces a quinonoid structure such as

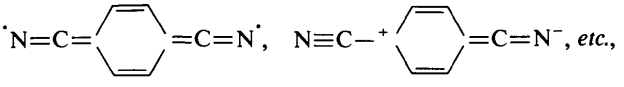

which implies greater π bonding in C(1′)–C(1) than in C(1)–C(2). In agreement with this interpretation, the width of the 0·1 e Å^{-3} contour perpendicular to the ring is 1·41 Å at the C(1′)–C(1) peak *vs* 1·28 Å for C(1)–C(2) (Fig. 5*c*,*d*). That this is a reasonable way to estimate the strength of π bonding is supported by the in-plane width of the same 0·1 e Å^{-3} contour, which should not be affected by π bonding and is found to be 0·89 Å for both bonds.

Further corroboration is provided by the shapes of the several peaks in the C–C≡N region of the molecule. In the exocyclic C(2)–C(3) bond, the 0·1 e Å^{-3} contour has an out-of-plane width of 1·02 Å, compared with 0·93 Å in the plane, supporting the suggestion of a partial π component in this bond. Conversely, the C≡N peak is wider in the plane than in the perpendicular direction, 1·30 *vs* 1·23 Å, as expected for a partially allenic (C=C=N) structure. Finally, the nitrogen lone-pair peak is, again, broader out-of-plane than in-plane, 0·95 *vs* 0·91 Å. Thus the contour maps fully support the proposed quinonoid bonding in this molecule.

But the inequality of bond lengths in the benzene ring could be simply a manifestation of the '*ipso*' effect described by Domenicano, Vaciago & Coulson (1975) and more quantitatively by Domenicano, Murray-Rust & Vaciago (1983). This causes the two bonds adjacent to a σ-electronegative substituent to be shortened and the angle between them widened. The atomic charges in Table 5 leave no doubt that F is the more electronegative of the two substituents. Assuming additivity of the effects of the several substituents, we expect that bond C(1′)–C(1), adjacent to two F substituents, should be shorter than C(1)–C(2), which lies between F and CN substituents, also that the ring angle at C(1) should be greater than that at C(2). Fig. 3 shows both these expectations to be fulfilled. However, if this were the main explanation for these effects, they should be reversed in terephthalonitrile (*p*-dicyanobenzene), which lacks the fluoro substituents. The structural evidence is clear but equivocal. Four crystallographic studies of terephthalonitrile (van Rij & Britton, 1977; Drück & Littke, 1979; Guth, Heger & Drück, 1982; Colapietro, Domenicano, Portalone, Schultz & Hargittai, 1984) and a gas-phase electron-diffraction study (Colapietro *et al.*, 1984) all agree that the ring angles at the substituted C atoms are, indeed, slightly larger than the others but that the bonds adjacent to the cyano substituents are, as in TFT, longer than the other two. It seems that the angular variation in terephthalonitrile is dominated by the *ipso* effect while the bond lengths are mainly sensitive to conjugation effects. In agreement with this interpretation, the angles opposite the F substituents in 2,3,5,6-tetrafluorobiphenyl (Goodhand & Hamor, 1978) average 121·7°, 1·2° greater than the corresponding angles in TFT, while the bond lengths show no clear sign of the *ipso* effect (but may perhaps have been inadequately corrected for libration).

A favored explanation for the *ipso* effect (Bent, 1961; Domenicano *et al.*, 1975) holds that the hybridization of a C atom bearing an electron-withdrawing substituent is altered so as to strengthen the adjacent σ bonds in the ring. This effect should, then, be revealed by enhanced bonding density, in the relevant bonds, in the plane of the ring. Fig. 5(*a*) indeed shows the deformation density in the C(1′)–C(1) bond to reach a peak of 0·76 e Å^{-3}, compared with 0·68 e Å^{-3} for C(1)–C(2). Thus it appears from the deformation density as well as from the structural evidence that quinonoid conjugation with the cyano groups and the σ-electronegativity of the F substituents both contribute to the observed inequality of bond lengths and angles in the benzene ring of TFT.

The net charges on C(1) and C(2) balance almost exactly the negative charges on the respective substituents F and CN (Table 5); *i.e.* the electron-withdrawing effect of the substituents is highly localized, with almost no sign of charge flow within the aromatic ring to equalize the charges on the ring atoms. This seems contrary to the accepted notion that inductive effects are readily transmitted through the delocalized π system.

The cyano group

The atomic moments in the CN fragment may be compared with values found in cyanoguanidine, $(NH_2)_2CNCN$ (Hirshfeld & Hope, 1980), and in pyridinium dicyanomethylide, $C_5H_5NC(CN)_2$ (Baert, 1979; Baert *et al.*, 1982) as well as with theoretical values in the molecules HCN, HCCCN, NCCN (Hirshfeld, 1977*b*), N_3CN and HCOCN (Eisenstein, 1981). Table 6 lists the atomic charges and moments in all eight CN groups. This extends and updates a more limited comparison by Moss (1982). For the three X-ray studies, the tabulated moments are based on the formal definition of the pseudomolecule in terms of the multipoles centered on the atoms of one molecule. In cyanoguanidine, the alternative definition based on the stockholder partitioning of the crystal density leads to a greatly reduced charge on the cyano N atom, −0·286 instead of −0·417 e. The large negative dipole and second moments on this atom are also drastically modified (to $\mu_l =$ +0·016 e Å, $\mu_{ll} = -0{\cdot}022$, $\mu_{mm} = \mu_{nn} = 0{\cdot}016$ e Å^2). The somewhat exaggerated sensitivity of these values to the crystal partitioning is attributable to the close interaction between N–H···N hydrogen-bonded molecules in this structure.

In six of the molecules listed in Table 6, the polarity of the C≡N bond, as measured by the difference $q_C - q_N$, is remarkably constant at 0·26 ± 0·01 e even though the total charge on the CN group, $q_C + q_N$, varies from 0 to −0·14 e. The only exceptions are the two molecules cyanogen azide and cyanoguanidine, in which the cyano group is linked to N, where $q_C - q_N$ rises to 0·35 or 0·47 e (the latter value dropping to 0·36 e with the stockholder partitioning). This greater polarity may be related to resonance, in these molecules, with structures containing an allenic $-N{=}C{=}N^-$ unit. In all cases examined the cyano C is characterized by a highly negative μ_l, due to polarization into the triple bond, more pronounced in the theoretical than in the experimental studies, and by positive μ_{mm} and μ_{nn}, indicating a transverse charge contraction or loss of π density. On N, the major feature is a negative μ_{ll}, implying longitudinal expansion; the tabulated moments also imply a moderate polarization into the lone-pair region and, in most cases, a slight transverse expansion, or gain of π density. An exceptional feature of the moments observed in pyridinium dicyanomethylide (Baert, 1979) is the extreme anisotropy in directions perpendicular to the C≡N bond; unlike all other molecules studied, where the in-plane and out-of-plane second moments μ_{mm} and μ_{nn} are nearly equal on both C and N atoms, here μ_{mm} is more positive than μ_{nn} by 0·13 and 0·10 e Å^2, respectively, on C and N. This anisotropy shows itself, in the static deformation maps of Baert *et al.* (1982), mainly in the zero contours.

On the whole, the three X-ray studies display a rather wider diversity in corresponding moments than the five SCF studies. This may arise from a greater uncertainty in the experimental values as well as an additional variability due to crystal effects. Before ascribing such differences to experimental aberrations, however, we should remind ourselves that these outer moments, in contrast to the contour maps, primarily emphasize diffuse features in peripheral regions where the nuclear attraction is weak, and these may be especially sensitive to mutual perturbation by neighboring groups in the same molecule as well as by intermolecular influences.

The C–F *bond*

For the C–F bond the only relevant comparison appears to be with the SCF calculation for formyl fluoride, HCOF (Eisenstein, 1981). The net charge on F is found to be virtually identical in the two molecules while the bond polarity $q_C - q_F$ varies from 0·255 to 0·433 e (Table 6). The two F atoms have very similar dipole moments, reflecting a backward polarization of their σ density (see below), and their second moments are uniformly small. On C, the obvious difference in molecular environments appears to express itself only in the π density. Thus, the greater positive charge in HCOF, 0·307 *vs* 0·126 e, is paralleled by a larger out-of-plane second moment μ_{nn}, 0·307 *vs* 0·200 e Å^2, evidence of a loss of π density to the carbonyl O atom; all in-plane moments are closely equal in the two molecules.

Table 6. *Net charges* ($\times 10^3$, e), *dipole moments* ($\times 10^3$, e Å), *and second moments* ($\times 10^3$, e Å^2) *of atomic deformation densities in several cyano groups, listed in order of increasingly negative group charge* $q_C + q_N$, *and in two* C–F *bonds*

On each atom the *l* axis is directed from C to N or F, *m* lies (in non-linear molecules) in or near mean molecular plane, *n* is perpendicular to both.

			C					N or F				
Molecule	Method	Ref.*	q	μ_l	μ_{ll}	μ_{mm}	μ_{nn}	q	μ_l	μ_{ll}	μ_{mm}	μ_{nn}
NCCN	SCF	(*a*)	126	−143	11	164	164	−126	−33	−104	−2	−2
$C_6F_4(CN)_2$	X-ray		113	−102	15	174	185	−151	−12	−51	12	22
HCCCN	SCF	(*a*)	96	−127	−18	117	117	−176	−35	−101	−30	−30
HCOCN	SCF	(*b*)	79	−141	5	161	152	−165	−34	−112	−30	−13
HCN	SCF	(*a*)	66	−161	46	149	149	−201	−45	−134	−37	−37
$C_5H_5NC(CN)_2$	X-ray	(*c*)	68	−87	−35	146	15	−205	−36	−72	−7	−103
N_3CN	SCF	(*b*)	100	−144	−41	142	127	−245	−47	−128	−44	−66
$(NH_2)_2CNCN$	X-ray	(*d*)	51	−92	−64	159	155	−417	−71	−105	−82	−89
HCOF	SCF	(*b*)	307	63	120	96	307	−126	−51	37	−8	0
$C_6F_4(CN)_2$	X-ray		126	67	110	87	200	−129	−60	13	5	11

* References: (*a*) Hirshfeld (1977*b*); (*b*) Eisenstein (1981); (*c*) Baert (1979); (*d*) Hirshfeld & Hope (1980).

A notable feature of the TFT deformation density, particularly emphasized by DSS, is the near absence of observable bonding density in the C–F bond. In the promolecule, composed of undeformed spherical atomic densities, the F nucleus would encounter an anti-binding or repulsive electric field of 0·322 e Å^{-2}, equal to the effect of a net positive charge of 0·57 e at the position of atom C(1). (1 e Å^{-2}, the field produced by a unit electronic charge at a distance of 1 Å, is $1{\cdot}4400 \times 10^{11}$ V m^{-1}.) Evidently, the diminutive peak of deformation density near the midpoint of the C–F bond (Fig. 5*a*, *e*), nothing like the size of the other bond peaks in this molecule, is hardly enough to provide the electrostatic balance demanded by the Hellmann–Feynman theorem. So what holds the F atom from flying off into space?

The shape of the observed deformation density near the F nucleus offers no hint of the answer. The major features are a pair of troughs on the bond axis, one in front of the nucleus and a smaller and shallower one behind, and a roughly disc-shaped peak perpendicular to the bond and centered on the nucleus. The overall effect suggests a depletion of a $2p_\sigma$ orbital along the bond axis and an enhancement of the two perpendicular $2p$ orbitals, as required formally to prepare the initially spherical atom for covalent bonding. Such a redistribution of charge among the atomic $2p$ orbitals would yield a totally centrosymmetric deformation density, producing no net field at the F nucleus. But Fig. 5 shows that the depleted σ function is far from a pure p orbital; rather it is strongly polarized into the bond as by s–p hybridization. The net effect is a removal of σ density mainly from the region in front of the nucleus and this is just the opposite of what is required to provide the binding field we are seeking. It seems the deformation density near the F nucleus reinforces the repulsive field due to the promolecule rather than countering it.

If we cannot recognize distinct features in the contour maps that might provide the required binding, we may look for a more diffuse migration of charge in the region surrounding the F nucleus. Thus, we have integrated the deformation density in a cylindrical region of 2·0 Å length and 1·5 Å radius centered on the nucleus with its axis along the C–F bond. The result is another disappointment. We find the forward half of this cylinder depleted of charge, by 0·21 e, while the region behind the nucleus contains a net excess of 0·15 e. The field at the nucleus produced by this charge displacement is anti-binding, with a value, derived by numerical integration, of 1·63 e Å^{-2}, *i.e.* five times the promolecule field and in the same direction. An almost identical result is obtained more simply by direct summation of the fields due to the polar (odd n) multipole functions centered on F, whose contribution far exceeds that of all functions on neighboring atoms. Each such function contributes a field, directed along its symmetry axis, equal to $\alpha_F^2/9$ for $n = 1$ or $\alpha_F^2/25$ for $n = 3$, multiplied by its experimentally determined coefficient. Vectorial summation of the appropriate terms leads to a net repulsive field of 1·59 e Å^{-2}, close to the value obtained by numerical integration. The experimentally derived deformation density simply does not satisfy the Hellmann–Feynman theorem.

The explanation of this result may be found in the theoretically calculated deformation density for formyl fluoride (Eisenstein & Hirshfeld, 1983). The contour maps in the neighborhood of the C–F bond are, as noted above, closely similar to those in Fig. 5. And a similar backward polarization of charge is found around the F atom, adding up to a net depletion of 0·17 e from a cylindrical region 1·0 Å long and 1·5 Å in radius surrounding the C–F bond, balanced by an excess of 0·15 e in a corresponding volume behind the F nucleus. Nevertheless, integration over the

deformation density in this cylindrical region yields an *attractive* field of about 0·034 e Å^{-2}. The source of this attraction is an extremely sharp forward polarization of charge in the immediate vicinity of the F nucleus, so sharp that the numerical integration is rather imprecise even on a grid of 0·005 Å near the nucleus. (This inner polarization is also poorly represented by the Gaussian basis, which helps to explain why the SCF calculation produces a severely non-zero value for the net Hellmann–Feynman field at the F nucleus : 0·300 in the promolecule minus 0·034 e Å^{-2} from the deformation density.) The field arising in this core region, within about 0·13 Å of the nucleus, is several times larger than that required to cancel the repulsion due to the promolecule but is largely offset by the repulsive field from more distant portions of the deformation density. This pattern is very similar to that found in the diatomic molecules HF and F_2, among others, where forward polarization of the near-in density was shown to be crucial for electrostatic binding (Hirshfeld & Rzotkiewicz, 1974). If we suppose that the situation in TFT is similar, it is obvious why we cannot obtain a sensible estimate of the Hellmann–Feynman field; the predominant contribution to this field arises in that very small region around the nucleus where our deformation density is completely unreliable.

An alternative and equally valid description of the C–F bond in formyl fluoride emerges from an orbital decomposition of the SCF deformation density into σ and π components. The π contribution to the field at the F nucleus, from the occupied π molecular orbitals minus corresponding π atomic orbitals, is found to be strongly attractive, with a value of 0·189 e Å^{-2}. This is opposed by a net repulsive σ contribution, in which the binding field from the core region is outweighed by a larger repulsion arising from the outer parts of the σ density. So the net binding can be attributed to forward polarization of the π density, partly offset by an anti-binding effect of the σ density. This, again, is analogous to the behavior in HF and F_2 (Hirshfeld & Rzotkiewicz, 1974). Unfortunately, no evidence for these opposing σ and π effects can be found in the overall deformation density. Even where the π density is greatest it is masked by a much larger σ density and cannot be separately distinguished. So this orbital analysis of the C–F bond is entirely theoretical and not subject to confirmation by an experimental deformation density.

The electrostatic equilibrium that maintains the stability of the C–F bond in TFT is, therefore, well understood from theoretical calculations on analogous molecules but completely unverifiable by X-ray diffraction.

It is a pleasure to thank Professor Jack Dunitz for supplying the highly dependable and carefully cross-checked X-ray data for this study and for patiently helpful stimulation and encouragement throughout. I am grateful also to Professor François Baert for unpublished results from his study of pyridinium dicyanomethylide.

References

BAERT, F. (1979). Personal communication.
BAERT, F., COPPENS, P., STEVENS, E. D. & DEVOS, L. (1982). *Acta Cryst.* A**38**, 143–151.
BENT, H. A. (1961). *Chem. Rev.* **61**, 275–311.
BUSING, W. R. & LEVY, H. A. (1964). *Acta Cryst.* **17**, 142–146.
COLAPIETRO, M., DOMENICANO, A., PORTALONE, G., SCHULTZ, G. & HARGITTAI, I. (1984). *J. Mol. Struct.* **112**, 141–157.
COPPENS, P. (1982). *Electron Distributions and the Chemical Bond*, edited by P. COPPENS & M. B. HALL, pp. 61–92. New York, London: Plenum.
DOMENICANO, A., MURRAY-RUST, P. & VACIAGO, A. (1983). *Acta Cryst.* B**39**, 457–468.
DOMENICANO, A., VACIAGO, A. & COULSON, C. A. (1975). *Acta Cryst.* B**31**, 221–234.
DRÜCK, U. & LITTKE, W. (1979). *Acta Cryst.* B**34**, 3095–3096.
DUNITZ, J. D., SCHWEIZER, W. B. & SEILER, P. (1982). *Helv. Chim. Acta*, **66**, 123–133.
EISENSTEIN, M. (1979). *Acta Cryst.* B**35**, 2614–2625.
EISENSTEIN, M. (1981). PhD thesis, Feinberg Graduate School, Weizmann Institute of Science.
EISENSTEIN, M. & HIRSHFELD, F. L. (1983). *J. Comput. Chem.* **4**, 15–22.
GOODHAND, N. & HAMOR, T. A. (1978). *Acta Cryst.* B**34**, 1644–1647.
GUTH, H., HEGER, G. & DRÜCK, U. (1982). *Z. Kristallogr.* **159**, 185–190.
HAREL, M. & HIRSHFELD, F. L. (1975). *Acta Cryst.* B**31**, 162–172.
HIRSHFELD, F. L. (1971). *Acta Cryst.* B**27**, 769–781.
HIRSHFELD, F. L. (1976). *Acta Cryst.* A**32**, 239–244.
HIRSHFELD, F. L. (1977*a*). *Isr. J. Chem.* **16**, 226–229.
HIRSHFELD, F. L. (1977*b*). *Theor. Chim. Acta*, **44**, 129–138.
HIRSHFELD, F. L. & HOPE, H. (1980). *Acta Cryst.* B**36**, 406–415.
HIRSHFELD, F. L. & RZOTKIEWICZ, S. (1974). *Mol. Phys.* **27**, 1319–1343.
MOSS, G. (1982). *Electron Distributions and the Chemical Bond*, edited by P. COPPENS & M. B. HALL, pp. 383–411. New York, London: Plenum.
REES, B. (1977). *Isr. J. Chem.* **16**, 180–186.
RIJ, C. VAN & BRITTON, D. (1977). *Acta Cryst.* B**33**, 1301–1303.
RIJ, C. VAN & BRITTON, D. (1981). *Cryst. Struct. Commun.* **10**, 175–178.
ROSENFIELD, R. E., TRUEBLOOD, K. N. & DUNITZ, J. D. (1978). *Acta Cryst.* A**34**, 828–829.
SEILER, P., SCHWEIZER, W. B. & DUNITZ, J. D. (1984). *Acta Cryst.* B**40**, 319–327.